THE JOURNAL OF BIOLOGICAL CHEMISTRY VOL. 281, NO. 49, pp. 37993–38003, December 8, 2006

Structural Characterization of Spo0E-like Protein-aspartic Acid Phosphatases That Regulate Sporulation in Bacilli*[S]

Received for publication, August 9, 2006, and in revised form, September 21, 2006 Published, JBC Papers in Press, September 25, 2006, DOI 10.1074/jbc.M607617200

Rosa Grenha[‡1], Neil J. Rzechorzek[‡], James A. Brannigan[‡2], Rob N. de Jong[§], Eiso AB[§], Tammo Diercks[§], Vincent Truffault[§3], Joanne C. Ladds[‡], Mark J. Fogg[‡], Cristina Bongiorni[¶], Marta Perego[¶], Robert Kaptein[§], Keith S. Wilson[‡], Gert E. Folkers[§4], and Anthony J. Wilkinson[‡]

From the [‡]Structural Biology Laboratory, Department of Chemistry, University of York, York YO10 5YW, United Kingdom, [§]Bijvoet Center, NMR Department, Utrecht University, 3584 CH Utrecht, The Netherlands, and the [¶]Division of Cellular Biology, Department of Molecular and Experimental Medicine, The Scripps Research Institute, La Jolla, California 92037

Spore formation is an extreme response of many bacterial species to starvation. In the case of pathogenic species of *Bacillus* and *Clostridium*, it is also a component of disease transmission. Entry into the pathway of sporulation in *Bacillus subtilis* and its relatives is controlled by an expanded two-component system in which starvation signals lead to the activation of sensor kinases and phosphorylation of the master sporulation response regulator Spo0A. Accumulation of threshold concentrations of Spo0A~P heralds the commitment to sporulation. Countering the activities of the sensor kinases are phosphatases such as Spo0E, which dephosphorylate Spo0A~P and inhibit sporulation. Spo0E-like protein-aspartic acid-phosphate phosphatases, consisting of 50–90 residues, are conserved in spore-forming bacteria and unrelated in sequence to proteins of known structure. Here we determined the structures of the Spo0A~P phosphatases BA1655 and BA5174 from *Bacillus anthracis* using nuclear magnetic resonance spectroscopy. Each is composed of two anti-parallel α-helices flanked by flexible regions at the termini. The signature SQELD motif (SRDLD in BA1655) is situated in the middle of helix α2 with its polar residues projecting outward. BA5174 is a monomer, whereas BA1655 is a dimer. The four-helix bundle structure in the dimer is reminiscent of the phosphotransferase Spo0B and the chemotaxis phosphatase CheZ, although in contrast to these systems, the subunits in BA1655 are in head-to-tail rather than head-to-head apposition. The implications of the structures for interactions between the phosphatases and their substrate Spo0A~P are discussed.

Spore formation is an extreme developmental response of many Gram-positive species of bacteria, exemplified by *Bacillus subtilis*, to nutrient deprivation (1). It starts with an asymmetric septation, which produces a larger mother cell and a smaller forespore. The mother cell engulfs the forespore and nurtures it during its development into a resistant spore. The spore is released in the final stages upon lysis of the mother cell and can remain dormant in the soil until favorable conditions for growth are restored and it can germinate. Spores are important in the life cycle of a number of human pathogens most notably in the food-borne agents *Clostridium botulinum* and *Bacillus cereus* and the anthrax agent *Bacillus anthracis* (2).

Sporulation is energetically expensive, requiring the activation of hundreds of hitherto silent genes at a time when nutrients are scarce. As a result, it is under elaborate control. At the heart of the regulatory system is an expanded two-component signal transduction system, termed the phosphorelay (3). The phosphorelay consists of multiple sensor kinases (4–6) that, when activated by appropriate environmental, metabolic, and cell cycle stimuli, autophosphorylate on a conserved histidine residue. The phosphoryl group is then relayed via an aspartate on Spo0F and a histidine on Spo0B to an aspartate on Spo0A. Spo0A is a response regulator and the master control element in the initiation of sporulation. If a threshold concentration of Spo0A~P is achieved, the cell is committed to the sporulation pathway. Attainment of this threshold requires elevated levels of *spo0A* expression as well as increased flux of phosphoryl groups through the phosphorelay. The latter requires not only elevated activity of the sporulation sensor kinases that feed the phosphorelay but also the inactivity of a number of protein-aspartic acid phosphatases that drain it (7–9).

Spo0F and the receiver domain of Spo0A have similar tertiary structures (10, 11). Each is capable of reversible phosphotransfer to Spo0B implying a similar phosphorylation site stereochemistry. Despite these similarities, the phosphatases that dephosphorylate Spo0F~P and Spo0A~P are quite different. The Rap phosphatases, RapA, RapB, and RapE, which are active

* This work was supported in part by the European Commission as SPINE Contract QLG2-CT-2002-00988 under the program "Quality of Life and Management of Living Resources" and Grant 87/C14673 from the Biotechnology and Biological Sciences Research Council. Work at The Scripps Research Institute was supported in part by NIGMS Grant GM55594 and NIAID Grant AI52289 from the National Institutes of Health. The oligonucleotide synthesis and DNA sequencing was supported in part by The Stein Beneficial Trust. The costs of publication of this article were defrayed in part by the payment of page charges. This article must therefore be hereby marked "*advertisement*" in accordance with 18 U.S.C. Section 1734 solely to indicate this fact.

[S] The on-line version of this article (available at http://www.jbc.org) contains supplemental Table S1 and Figs. S1 and S2.

The atomic coordinates and structure factors (codes 2BZB and 2C0S) have been deposited in the Protein Data Bank, Research Collaboratory for Structural Bioinformatics, Rutgers University, New Brunswick, NJ (http://www.rcsb.org/).

[1] Co-financed by the Fundação para a Ciência e a Tecnologia, Portugal, by Grants POCI2010 and Fundos Comunitários.

[2] Supported by the Wellcome Trust. To whom correspondence may be addressed. Tel.: 44-1904-328271; Fax: 44-1904-328266; E-mail: jab@ysbl.york.ac.uk.

[3] Present address: Max Planck Institute for Developmental Biology, Dept. of Protein Evolution, Spemannstrasse 35, 72076 Tübingen, Germany.

[4] To whom correspondence may be addressed. Tel.: 31-30-2539930; Fax: 31-30-2537623; E-mail: g.folkers@chem.uu.nl.

Supplemental Material can be found at: http://www.jbc.org/cgi/content/full/M607617200/DC1

against Spo0F~P, have molecular masses of ~45 kDa and contain six tetratricopeptide repeats (12). Their activities are regulated by peptides derived from downstream Phr proteins following an export-import maturation process (13). In contrast Spo0E, YisI, and YnzD, which dephosphorylate Spo0A~P, are small 50–90-residue proteins, and little is known about their regulation (9).

Structural studies of the components of the phosphorelay have provided important insights of wider significance including (i) the first glimpse of phosphorylated aspartic acid in a protein and the associated stereochemistry that is conserved across the response regulator family (10) and (ii) the first view of a complex between a response regulator and a sensor kinase-type phosphotransferase domain, placing studies of the evolution of protein recognition in two-component systems on a firm footing (14). To complement and extend these studies, structures of the kinases and phosphatases that feed and drain the sporulation phosphorelay are needed. We have attempted, without success, to crystallize the Spo0E, YisI, and YnzD proteins from *B. subtilis*. We therefore extended our study to putative Spo0A~P phosphatases from *B. anthracis*. In this organism, the major components of the sporulation phosphorelay, Spo0F, Spo0B, and Spo0A, are essentially identical (15), although they may be phosphorylated by as many as nine sensor histidine kinases (16). Two putative Spo0E-type proteins, BA1655 and BA5174, were purified and shown to have Spo0A-phosphate phosphatase activity. With crystals continuing to prove elusive, we used nuclear magnetic resonance spectroscopy to determine the structures of both proteins. The structures provide insights into the Spo0E-dependent dephosphorylation of Spo0A, the master regulator of sporulation.

EXPERIMENTAL PROCEDURES

Cloning and Expression—DNA fragments encoding BA1655 and BA5174 were amplified by PCR from *B. anthracis* UM23CL-2 genomic DNA. Sequence alignment data showed that the annotated sequences provided by The Institute for Genomic Research (Rockville, MD) for the loci BA5174 and BA1655 may possess 51 and 18 extra residues, respectively, at their N termini compared with *B. subtilis* Spo0E. The coding sequences for these "extra" amino acid residues were omitted from the final constructs used in this work. The amplified fragments were digested with the restriction endonucleases NcoI and XhoI and ligated to similarly cut pET-28a vector DNA (Novagen). The ligation products were introduced into *Escherichia coli* NovaBlue competent cells (Novagen). Restriction enzyme digestion analysis of recombinant plasmids and subsequent DNA sequencing allowed the isolation of desired recombinants in which the coding sequences of the phosphatases are placed adjacent to a sequence encoding a C-terminal hexahistidine tag (LEHHHHHH).

Protein Production—Protein expression and purification, as well as sample preparation, were performed as described previously (17). For production of ^{15}N-labeled protein, recombinant plasmids were introduced into *E. coli* BL21 (DE3) and grown at 37 °C in 500 ml of minimal medium (18) containing 4 g/liter glucose and 0.5 g/liter $^{15}NH_4Cl$. At an OD_{600} of 0.5, protein expression was induced by the addition of isopropyl thio-β-D-galactopyranoside to a final concentration of 0.5 mM, and the culture was incubated with shaking at 30 °C for a further 4 h. $^{13}C/^{15}N$ doubly labeled protein was prepared in the same way with [^{13}C]glucose at 2 g/liter replacing the unlabeled glucose in the minimal medium.

Cells were harvested by centrifugation and resuspended in 10 ml of Buffer A (50 mM sodium phosphate, pH 8, 300 mM NaCl) containing 10 mM imidazole, 1 mM β-mercaptoethanol, 0.2 mM phenylmethylsulfonyl fluoride, 1 μg/ml lysozyme, and 1% (v/v) protease inhibitor mixture (Complete, Roche Applied Science) and frozen at −80 °C overnight. Following cell lysis by sonication, the soluble cell fraction was fractionated by Ni^{2+}-nitrilotriacetic acid chromatography using a Poros MC column and a BioCad Vision HPLC[5] system (Applied Biosystems). Samples were loaded in Buffer A containing 20 mM imidazole, and after washing, bound proteins were eluted in Buffer A containing 500 mM imidazole and directed onto a Sephadex G75 gel filtration column pre-equilibrated in 50 mM sodium phosphate, pH 8.0, 150 mM NaCl. Protein fractions eluting from this column were buffer-exchanged into 50 mM sodium phosphate buffer, pH 6.0, 150 mM NaCl in the case of BA5174 and 10 mM sodium phosphate, pH 6.0, 50 mM NaCl in the case of BA1655. The protein samples were concentrated initially to 0.3–1.0 mM, and sodium azide and D_2O were added to the samples to final concentrations of 0.02 and 10%, respectively.

NMR Spectroscopy—All NMR measurements on U-^{15}N- and U-^{13}C,^{15}N-labeled BA1655 and BA5174 were recorded on Bruker Avance spectrometers operating at 700 and 900 MHz. For the intrinsically dimeric BA1655, the temperature was set to 298 K, whereas a lower temperature of 278 K was chosen for BA5174 to obtain a homogeneous monomeric spectrum (see below). The three-dimensional spectra required for resonance assignment and structure determination were recorded using a standard set of NMR experiments (19). To accelerate resolution sampling in the indirect ^{15}N dimension, extensive spectral folding was applied resulting in sweep widths of 13.8 ppm for BA5174 and 7.0 ppm for BA1655. For resonance assignment of both proteins, we recorded slightly different sets of NMR spectra to account for the substantially lower inherent sensitivity of the BA5174 sample (~0.3 mM concentration at 278 K) compared with the BA1655 sample (~1 mM dimer concentration at 298 K). Thus, for both samples we recorded sequential CO and CA information for backbone assignment in three-dimensional inter-residual ($i - 1$) HNCO and CBCA[CO]NH and bifurcate (i, $i - 1$) HN[CA]CO and HNCA experiments as well as side chain information in three-dimensional [H]CCH correlated spectroscopy, H[C]CH total correlated spectroscopy, and [H]C[CCO]NH total correlated spectroscopy experiments. The optional, more sensitivity-limited three-dimensional (i, $i - 1$) HNCACB (to obtain sequential CB information) and H[CCO]NH total correlated spectroscopy experiments for backbone and side chain assignment, respectively, were only recorded for BA1655. For BA5174, we recorded instead three-

[5] The abbreviations used are: HPLC, high pressure liquid chromatography; NOE, nuclear Overhauser enhancement; r.m.s., root mean square; N-Spo0A, the receiver domain of Spo0A; BA, *B. anthracis*; FPLC, fast protein liquid chromatography; GAP, GTPase-activating protein.

dimensional ($i - 1$) HBHA[CO]NH and (i, $i - 1$) HN[CA]HA spectra to add sequential HA information to the backbone assignment protocol; we furthermore recorded a two-dimensional H,H total correlated spectroscopy experiment with H[^{15}N] suppression in the direct dimension (20) to better resolve and assign the additional six tyrosine aromatic moieties. All spectra were processed in XWinNMR 3.5 (Bruker Biospin, Rheinstetten, Germany), and peak lists were generated by SPARKY (21). Sequential backbone assignment was performed largely automatically using both PASTA (22) and AutoAssign (23), whereas manual side chain assignment was supported by in-house software. For structure elucidation we recorded a set of three-dimensional H,NH-, H,CH-, and [H]C,NH-NOE spectroscopy spectra (24) complemented by a high-resolution two-dimensional H,H-NOE spectroscopy spectrum. Automated NOE assignment and structure calculations were performed using the CANDID (25) module of CYANA2.1 (26), although NOE spectra were manually checked for $i + 3$ and $i + 4$ peaks to identify helical boundaries. Dihedral angle restraints were calculated using TALOS (27). Finally, water refinement was performed using CNS (28) according to the RECOORD protocol (29). Structures were validated using WHATIF (30) and PROCHECK (31, 32).

Molecular Weight Determination—Proteins were analyzed by gel filtration on a Superdex S75 column (3.2 × 30 cm) equilibrated and run using an FPLC system (Amersham Biosciences) at a flow rate of 1 ml/min in 50 mM sodium phosphate buffer, pH 7.6, containing 150 mM NaCl. Sedimentation equilibrium experiments were performed on a Beckman Optima XL/I analytical ultracentrifuge using Beckman cells with 12-mm path length double sector six-channel charcoal-filled Epon centerpieces and quartz windows in an AN-50Ti rotor. BA1655 (165 μg/ml) was prepared in 25 mM Tris, pH 8.0, 30 mM NaCl, whereas BA5174 (86 μg/ml) was prepared in 25 mM Tris, pH 8.0, 150 mM NaCl. Serial 2-fold dilutions of the protein were prepared, and 118 μl samples were centrifuged along with buffer samples as references at 25,000 rpm for 17 h and at 35,000 rpm for a further 18 h at 20 °C. The temperature was lowered to 8 °C, and runs at 35,000 rpm for 15 h and 25, 000 rpm for 21 h were performed. Radial absorbance scans were taken at 280 or 230 nm at ~3-h intervals until sedimentation equilibrium was achieved as judged by the absence of change in overlays of successive scans. The data were analyzed using the Beckman Origin software (supplied with the machine). A narrow range of data points around a series of radial points in the scan were used to estimate midpoint molecular weights using the Lamm equation for a single species. These were then plotted against concentration. The data were also analyzed by nonlinear least squares fitting to each set of data assuming a single species model (Beckman Origin software).

Protein concentrations were estimated as follows. For BA5174, the protein concentration was determined from plots of A_{280} *versus* A_{230} from scans taken at equilibrium at 35,000 rpm. These gave linear plots that indicated that $A_{280} = 0.109 \times A_{230}$. Thus, using the calculated A_{280} for 1 mg/ml protein = 0.563, 1 A_{230} (in a 1.2-cm path length cell) corresponds to 0.162 mg/ml (20 μM). For BA1655, which lacks Trp and Tyr residues and has a negligible extinction coefficient, the concentration was estimated from interference optical data assuming BA1655 gives a normal response. 1 A_{230} corresponds to 0.35 mg/ml protein.

In Vivo Assays—The BA1655 locus was cloned as a 380-bp fragment obtained by PCR amplification using the oligonucleotide primers BA1655–5′Eco (GAGCCGAATTCTTTTGTAATTAGACACACGC) and BA1655–3′BamII (TAAAAGGATCCAAATTCTTATTTATGTAC). This fragment included 207 bp upstream of the codon for the first methionine residue shown in Fig. 1. The fragment was cloned in the multicopy vector pHT315 (33). After propagation in the *dam*$^-$ *E. coli* strain C600, the resulting plasmid, pHT315-1655, was used to transform the *B. anthracis* Sterne strain 34F2 by the method of Koehler *et al.* (34). The phenotype of the transformants was analyzed on Schaeffer's sporulation agar plates (sporulation medium) (35). Transcription analysis was carried out by means of β-galactosidase assays on a *B. anthracis* 34F2 strain carrying a transcriptional *lacZ* fusion construct generated on plasmid pTCVlac (36). The 285-bp fragment containing the promoter region was generated by PCR amplification using oligonucleotide primers BA1655–5′Eco (see above) and BA1655–3′BamI (TATCAGGATCCAATCCATGTCTAGC). Strains were grown in liquid sporulation medium supplemented with 7.5 μg/ml kanamycin. Aliquots were taken at hourly intervals, and β-galactosidase activity was assayed as described previously (37) with the following modifications. The incubation at 37 °C with lysozyme was carried out for 1 h and Triton was used at 0.5% final concentration.

Activity Assays—The phosphorylated form of the receiver domain of Spo0A from *Bacillus stearothermophilus*, prepared as described previously (38), was generously provided by Dr. Rick Lewis, University of Newcastle-upon-Tyne. Its dephosphorylation by BA1655 and BA5174 was monitored using a gel electrophoresis assay exploiting the observation that dephosphorylation of N-Spo0A~P is associated with an increase in gel mobility (39, 40). In a buffer containing 25 mM Tris-HCl and 150 mM NaCl, N-Spo0A~P at a concentration of ~30 μM was incubated with 2-fold serial dilutions (3.6 μM to 60 nM) of BA1655 and BA5174. After 1 h at room temperature, a half-volume of sample buffer (1.5 M Tris-HCl, pH 8.8, 20% (v/v) glycerol, 0.1% (w/v) bromphenol blue) was added, and the samples were immediately loaded on a 12.5% non-denaturing polyacrylamide gel. Following electrophoresis at 150 V for 1.5 h at 4 °C, the proteins were visualized by Coomassie Blue staining.

RESULTS

The Distribution of Spo0E-like Phosphatases—The *spo0E* gene of *B. subtilis* was discovered following the characterization of strains in which sporulation was arrested at stage 0. The mutant phenotype was found to be due to Spo0E hyperactivity (8, 41). Subsequent analysis of the genome sequence of this organism led to the identification and characterization of two homologous proteins, YnzD and YisI, which dephosphorylate Spo0A~P and whose overexpression lowers the sporulation frequency (9).

Analysis of the genome sequences of *Bacillus* species in the Cereus group (*B. anthracis*, *B. cereus*, and *Bacillus thuringiensis*) suggests that there has been an expansion in the number of open reading frames that encode small protein-aspartate phos-

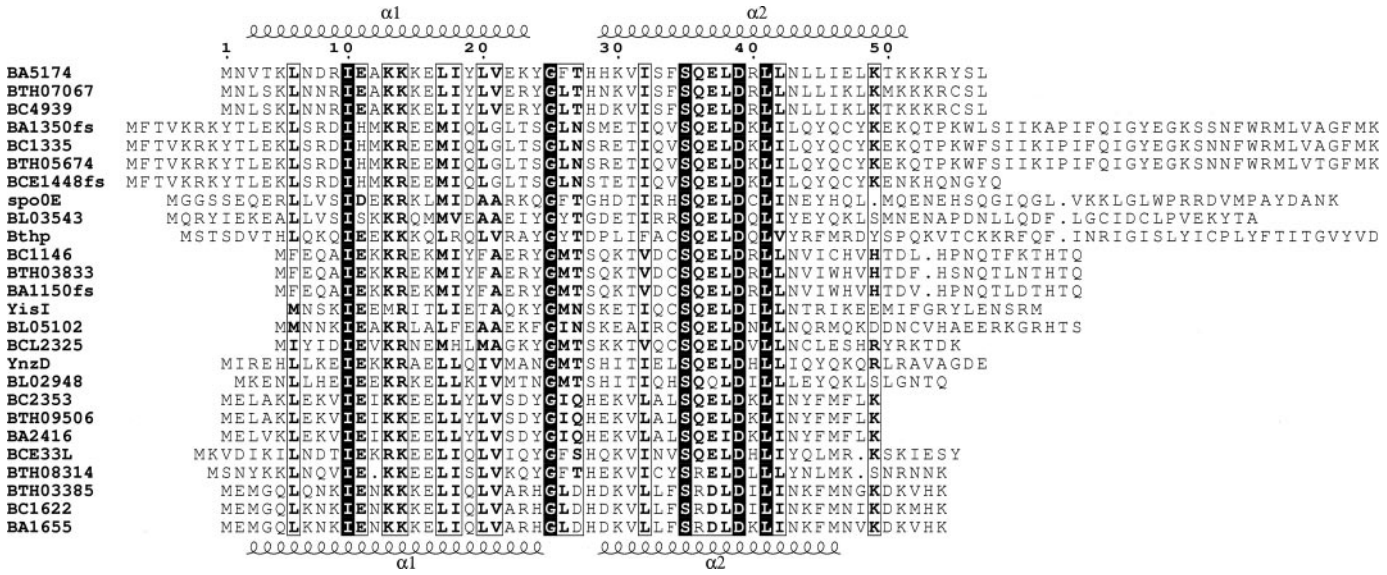

FIGURE 1. **The sequences of the three aspartic acid phosphatases of *B. subtilis* (Spo0E, YisI, and YnzD) aligned with predicted proteins from the mesophile *Bacillus licheniformis* and from members of the *B. cereus* group.** *BA*, *B. anthracis* Ames; *BC*, *B. cereus* ATCC 14579; *BLI*, *B. licheniformis* ATCC 14580; *BTH*, *B. thuringiensis israelensis* ATCC 35646. *Bthp* and *BCE33l* are previously unannotated genes encoded by megaplasmids. The secondary structure elements of BA5174 (*top*) and BA1655 (*bottom*) are shown. The figure was drawn using ESPript (50).

phatases. In *B. anthracis*, there appear to be five proteins with sequences resembling the Spo0E, YnzD, and YisI proteins of *B. subtilis*, although two in the Ames strain may not be functional due to frameshifts (supplemental Table S1). *B. cereus* also appears to have five *spo0E*-like genes, and *B. thuringiensis* may have six (supplemental Table S1). Large plasmids contained in *B. cereus* and *B. thuringiensis* also harbor homologous genes. A sequence alignment (Fig. 1) highlights the canonical "signature" sequence, SQELD*X*L (9). The first, fifth, and seventh residues are invariant with limited Gln → Arg, Glu → Gln/Asp, and Leu → Ile variations at the second, third, and fourth positions, respectively. These variations become more marked in the homologous proteins of a wider set of Gram-positive organisms that contain Spo0A-like substrate proteins, particularly those that live in extreme environments (supplemental Fig. S1).

BA1655 and BA5174 Dephosphorylate Spo0A in Vivo and in Vitro—To characterize further the Spo0E family of aspartic acid-phosphate phosphatases, we expressed and purified a number of Spo0E-like proteins from different *Bacillus* species. The *B. anthracis* proteins BA5174 and BA1655 were chosen for extended study because (i) both proteins could be overproduced in good yield and at high solubility from *E. coli*, and (ii) they are representative of Spo0E-like proteins that harbor the signature sequence SQELD*X*L (BA5174) and those that contain the most common variation on this motif, SRDLD*X*L (BA1655).

To determine whether these proteins play a role in regulating the sporulation phosphorelay, the genes encoding the BA1655 and BA5174 proteins were cloned on the multicopy vector pHT315 and transformed in the parental *B. anthracis* strain 34F2. Overexpression of Spo0E-like proteins results in a sporulation-deficient phenotype (Spo$^-$) due to their dephosphorylating activity on Spo0A~P (9). The *B. anthracis* strain carrying pHT315-1655 clearly showed a Spo$^-$ phenotype when grown on Schaeffer's sporulation medium compared with the strain carrying the vector alone (Fig. 2*A*). This result indicated that BA1655 is indeed a negative regulator of sporulation. Transcription analysis by means of β-galactosidase assays on a strain carrying a promoter *lacZ* fusion construct showed that a 207-bp fragment upstream of the coding sequence is sufficient to promote a relatively high level of expression that appeared to be essentially constitutive throughout the growth cycle (Fig. 2*B*). Similar *in vivo* analyses of BA5174 indicated that this gene is not transcribed at sufficiently high levels to result in overproduction of its gene product, thus explaining the lack of a sporulation phenotype when cloned on pHT315.[6]

Purified BA1655 and BA5174 were each able to promote the dephosphorylation *in vitro* of the phosphorylated form of the receiver domain of Spo0A (N-Spo0A) from *B. stearothermophilus*. Phosphorylated N-Spo0A has a lower electrophoretic mobility than the unphosphorylated protein in non-denaturing gels (40). As shown in Fig. 2*C*, incubation of N-Spo0A~P with either BA1655 or BA5174 led to an increase in mobility, confirming the capacity of both proteins to dephosphorylate N-Spo0A~P. BA5174 exhibited ~8-fold higher specific activity than BA1655 in these assays, an observation we made with two different protein preparations. To gain insights into the mechanism and substrate specificity of these small aspartic acid phosphatases, we determined the structures of these two representative members.

NMR Data and Structure Determination—As a step toward structure determination, we expressed and purified a number of Spo0E-like proteins from different *Bacillus* species in an unsuccessful quest for crystals. In the absence of crystals, we turned to NMR spectroscopy. The initial ^{15}N heteronuclear single quantum correlation spectra for both BA1655 and

[6] C. Bongiorni and M. Perego, manuscript in preparation.

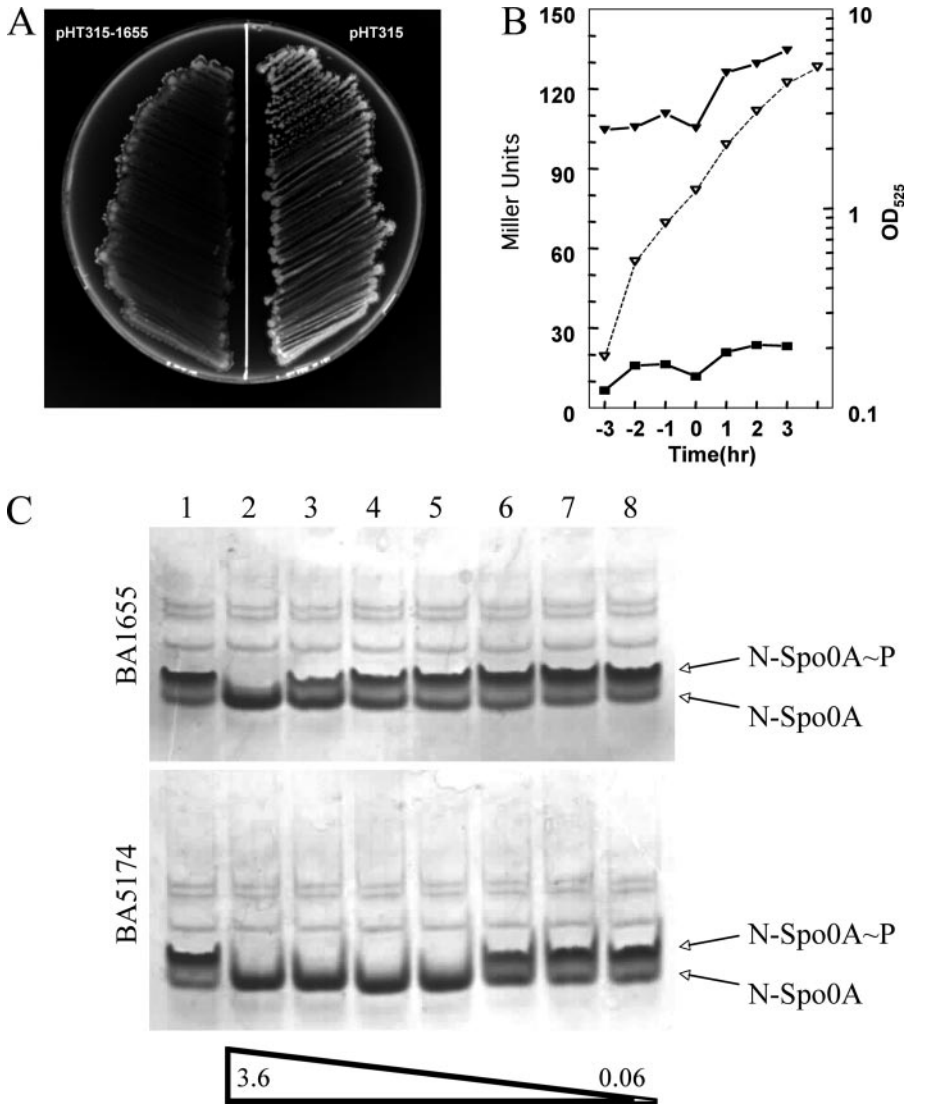

FIGURE 2. **Activity of *B. anthracis* phosphatases *in vivo* and *in vitro*.** *A*, sporulation-deficient phenotype of strain 34F2 carrying the pHT315-1655 plasmid (*streak* on the *left*) compared with parental strain carrying the pHT315 vector alone (*streak* on the *right*). Sporulation inhibition results in a transparent phenotype (*left*), whereas spore formation gives rise to an *opaque* (*white* appearance) streak (*right*). Strains were grown on Schaeffer's sporulation agar medium. *B*, time courses of β-galactosidase activity of the BA1655 promoter. $t = 0$ marks the transition between vegetative growth and the sporulation phase. ■, 34F2 control strain carrying the pTCVlac vector; ▼, 34F2 carrying pTCVlac-1655; ▽, growth curve of 34F2/pTCVlac-1655. Strains were grown in Schaeffer's sporulation broth. *C*, Spo0A-phosphate phosphatase activity assays. Shown are Coomassie Blue-stained 12.5% non-denaturing polyacrylamide gels loaded with samples containing 30 μM N-Spo0A~P (*lane 1*) and 30 μM N-Spo0A~P following incubation with 3.6, 1.8, 0.9, 0.45, 0.23, 0.11, and 0.06 μM (*lanes 2–8*) BA1655 (*upper panel*) and BA5174 (*lower panel*). Following dephosphorylation, the mobility of the N-Spo0A species increases.

BA5174 showed limited H^N dispersion (~7.1–8.8 ppm), characteristic of all α-helical proteins (supplemental Fig. S2). The BA5174 heteronuclear single quantum correlation spectra, however, revealed remarkable temperature dependence (data not shown) with a second set of signals appearing above 283 K and predominating at higher temperatures (>308 K). The disappearance of this second set of signals, with distinctly larger line widths, upon 10-fold dilution (to ~50 μM) at 298 K suggested reversible, yet stable multimerization. However, we cannot exclude the possibility that under these conditions aggregation accompanied by partial unfolding is occurring given the appearance of amide resonances around the random coil position together with the decrease in signal intensity for the monomeric species. We therefore chose to simplify the NMR investigations by carrying out experiments at the relatively low protein concentration of ~0.3 mM and at the lower temperature of 278 K at which a single species was prevalent. Even under these conditions, several heteronuclear single quantum correlation peaks from BA5174 either had shoulders or could be resolved into weak nearby second peaks, indicating the persistence of some conformational heterogeneity.

Complete sets of NMR spectra for assignment and structure elucidation were recorded in 15 and 22 days for BA1655 and BA5174, respectively, on spectrometers operating at 700 and 900 MHz ^1H frequency. These high field strengths offered crucial gains in resolution as both proteins display the rather low H^N and H^α frequency dispersion that is typical of all-helical proteins. A high proportion of α-helical structure was further indicated by the observation that all the H^α protons resonate below the water frequency (<4.7 ppm) and eventually proven by the final structure calculations from NOE data. It became clear that BA1655 forms dimers as the assumption that all the observed NOE distance restraints were *intra*molecular produced a pair of improbably bent helices. Canonical helices emerged only after allowing for the possibility that some of the observed NOE contacts were *inter*molecular. The observed single set of heteronuclear single quantum correlation signals irrespective of the chosen temperature (280–310 K) and concentration (0.5–1.5 mM) thus reflects a symmetric dimer state that is stable on the NMR time scale.

Structures of BA1655 and BA5174—Views of the ensemble of NMR structures for BA1655 and BA5174 along with a ribbon representation of the lowest energy structures are shown in Fig. 3, *A–D*. Data and statistics for the structures are presented in Table 1. Under the conditions used for the NMR experiments (protein concentration <0.5 mM and $T < 280$ K), BA5174 is a monomer composed of a pair of antiparallel α-helices joined by a short turn facilitated by the conserved Gly^{25} residue (Fig. 3, *A* and *B*). The two α-helices are closely packed with hydrophobic side chains on each helix intercalating in a manner reminiscent of other closely packed helical substructures such as leucine

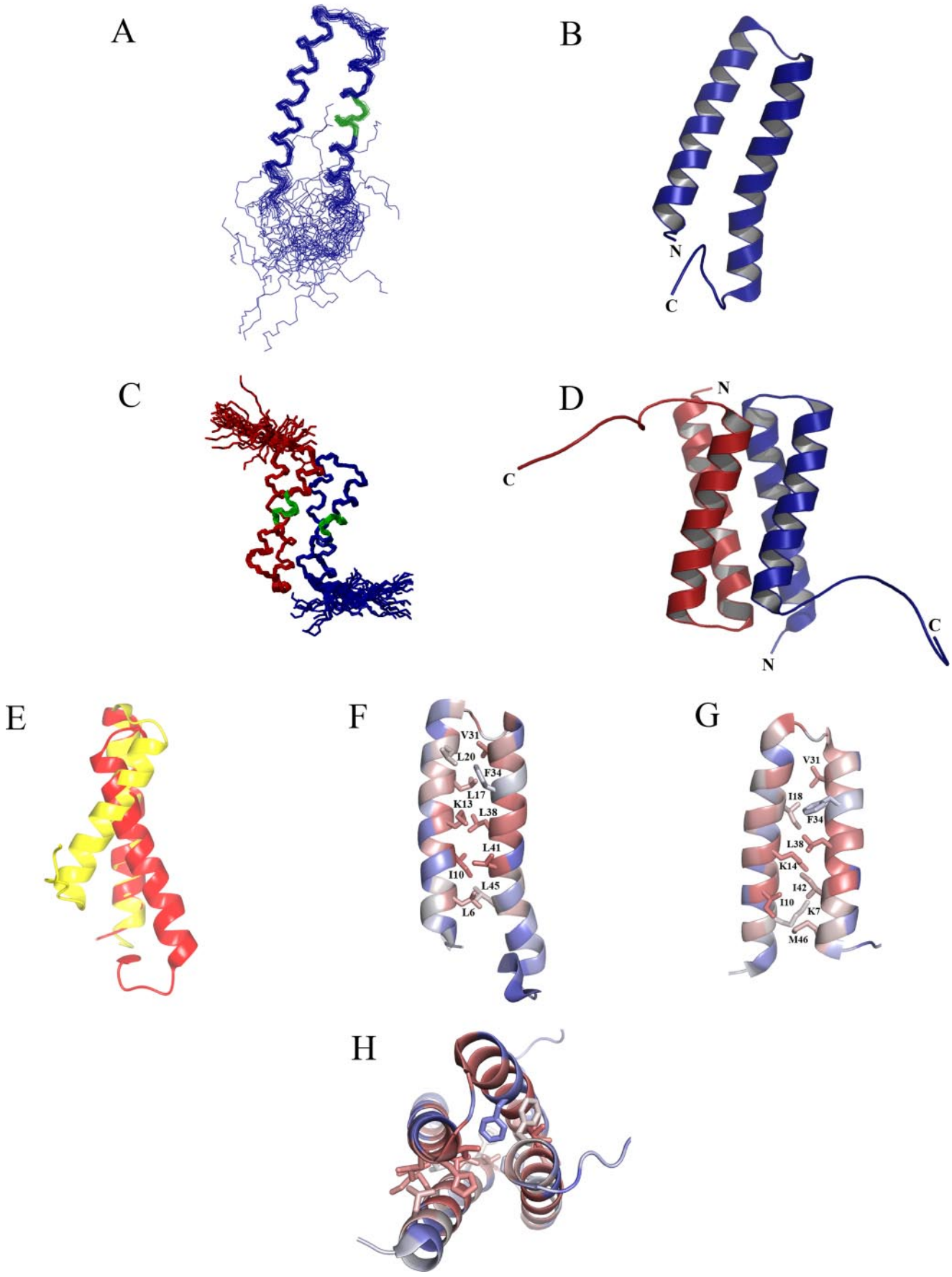

zippers. The helices are antiparallel to one another (Fig. 3). BA1655 consists of a similar pair of α-helices connected by an abrupt turn. In contrast to BA5174, at 298 K and at a protein concentration >0.5 mM BA1655 is a dimer (Fig. 3, *C* and *D*). In the dimer, the subunits pair in a head-to-tail orientation to form a four-helix bundle. The C-terminal residues including the hexahistidine tag are disordered.

Following least squares superposition of the Cα atoms of residues 4–47, which encompass the two helices, from one chain of BA1655 onto the equivalent atoms of BA5174, the root mean square (r.m.s.) deviation in Cα positions is 4.8 Å. This large r.m.s. deviation is the result of different helical orientations in the two proteins (Fig. 3*E*). The *intra*molecular packing of the helices is more extensive in BA5174 than in BA1655, compensating in part for the absence of surface area buried by *inter*molecular interactions. The helices wrap around one another to a greater extent in BA5174 so that *intra*molecular helix-helix packing buries ~1000 Å^2 of molecular surface area. In BA1655 a smaller surface area of 660 Å^2 is buried by α1-α2 interactions. In both proteins, ~90% of the atoms contributing to this interface are non-polar. In BA5174, the principal residues that form the interacting surface between the helices are Leu^6, Ile^{10}, Lys^{13}, Leu^{17}, and Leu^{20} from α1 and Val^{31}, Phe^{34}, Leu^{38}, Leu^{41}, and Leu^{45} from α2 (Fig. 3*F*). In BA1655, Lys^7, Ile^{10}, Lys^{14}, Ile^{18}, Val^{31}, Phe^{34}, Leu^{38}, Ile^{42}, and Met^{46} are the main contributors to helical packing (Fig. 3*G*).

In BA1655, ~2200 Å^2 of accessible surface area is buried in the dimer interface. Residues of BA1655 that contribute in excess of 50 Å^2 of surface area to this interface are Leu^6, Lys^{13}, Leu^{17}, Leu^{20}, Val^{21}, His^{24}, Phe^{34}, Leu^{41}, and Phe^{45} (Fig. 3*H*). 76% of the atoms contributing to this interface are hydrophobic. This is higher than is typical for surfaces involved in reversible interactions between proteins (42). It is not immediately obvious why BA1655 should be a dimer whereas BA5174 is a monomer. Among the residues interacting across the dimer interface in BA1655, the following residues differ in BA5174: His^{24} (Tyr^{24} in BA5174), which interacts with Met^{46} (Ile) and Leu^{26} (Phe), which interacts with Phe^{45} (Leu). These appear to be modest changes in sequence. It may be that differences in the residues that make up the loop between α1 and α2 influence the helical orientation and thus dimer formation.

The Conserved Motif—The ^{35}SQELD*X*L^{41} motif in BA5174 is situated toward the center of helix α2 (Fig. 4, *A* and *B*). The Ser^{35} side chain is oriented back along the helix so that (i) it is partially covered by the side chain of Phe^{26} and (ii) in ~50% of the structures within the ensemble the -OH group forms a hydrogen bond with the carbonyl oxygen of Val^{31}. The side chains of Gln^{36} and Asp^{39} project outward from the face of α2 that is distal to helix α1 with neither forming any intramolecular interactions. The side chain of residue Glu^{37} also projects outward from the molecule, although in this case it forms a salt-bridging contact in 50% of the structures with the side chain of Lys^{13} from helix α1. This lysine is well conserved in the sequences of the Spo0E-type phosphatases (Fig. 1), often occurring as one of a string of three consecutive positively charged residues. The side chains of the two conserved leucines, Leu^{38} and Leu^{41}, are at the core of the hydrophobic interactions between the two helices, forming contacts with numerous residues and playing an important structural role. As shown in Fig. 4*C*, the motif is surrounded by a surface of the molecule that is well conserved in the Spo0E protein family.

In BA1655, there are similarities and differences in the orientation and interactions of the side chains of the residues of the modified motif, ^{35}SRDLD*X*L^{41} (Fig. 4, *D*–*F*). Thus, as in BA5174 (i) the Ser^{35} hydroxyl forms a hydrogen bond with the main chain carbonyl oxygen of Val^{31} (although in BA1655 this hydrogen bond is present in all structures in the ensemble); (ii) Arg^{36}, Asp^{37}, and Lys^{40} project outward, although in 20% of the structures the latter pair makes a salt bridge; and (iii) the side chain of the Leu^{38} residue forms extensive interactions with helix α1. Otherwise the stereochemistry is altered because the α1-α2 juxtaposition is different in BA1655, and BA1655 is a dimer. The pair of motifs in the dimer forms a contiguous surface. The side chains of Asp^{39} form ionic interactions with the Lys^{14} side chains from helix α1 of the partner molecule in the dimer. The side chain of Leu^{41} contributes to the hydrophobic core of the molecule interacting extensively across the dimer interface.

Analytical Ultracentrifugation Confirms That BA1655 Is Dimeric, whereas BA5174 Is Monomeric—The unexpected difference in the quaternary structures of BA1655 and BA5174 and the temperature and concentration dependence of the line widths in the NMR spectra prompted us to examine the hydrodynamic properties of the two proteins using analytical ultracentrifugation. Sedimentation equilibrium experiments were performed at 25,000 and 35,000 rpm over a 10–20-fold range of starting concentrations, 1.9–22 μM for BA1655 and 0.5–10 μM for BA5174 at 8 and 20 °C. Plots of apparent molecular mass *versus* concentration are shown in Fig. 5. There is little or no concentration or temperature dependence of the apparent molecular mass of either protein, which was in the range of 14,500–15,200 Da for BA1655, whereas that of BA5174 was found to be between 8,200 and 8,600 Da. As the calculated molecular weight of BA1655 is 7,494 and that of BA5174 is 7,943, we conclude that BA1655 is a dimer and that BA5174 is a monomer. The data provide no evidence of monomer-dimer equilibration on the time scale of the experiment.

FIGURE 3. **The structures of *B. anthracis* BA5174 and BA1655.** *A* and *C*, superposition of 25 and 32 calculated NMR structures for BA5174 and BA1655, respectively. For the latter the individual monomers are colored *red* and *blue*. The SQELD and SRDLD motifs are highlighted in *green*. *B*, ribbon view of the lowest energy structure for BA5174 (Protein Data Bank code 2C0S) with C and N termini labeled. *D*, ribbon view of the lowest energy BA1655 structure (Protein Data Bank code 2BZB) with C and N termini labeled. Individual monomers are colored *green* and *blue*. The images were created using MOLMOL (51). *E*, the relative orientations of the helices in BA5174 (*red*) and the subunit of BA1655 (*yellow*). The structures were overlaid by least squares methods applied to the Cα atoms of the first α-helix (residues 2–24). The different orientation of the second helix in each structure is apparent. *F* and *G*, ribbon representations of BA5174 and a subunit of BA1655, respectively, with the side chains of residues participating in helix-helix interactions drawn in stick format and colored according to the extent of their conservation (*red-white-blue* as conservation decreases) in the alignment shown in Fig. 1 as determined in the program CONSURF (52). *H*, ribbon representation of the BA1655 dimer with the side chains of residues participating in dimer formation drawn in stick format and colored as above.

TABLE 1
Summary of structural constraints and structure statistics

	BA1655	BA5174
NOE-based distance restraints		
Intraresidue ($\|i-j\|=0$)	875	335
Sequential ($\|i-j\|\leq 1$)	773	255
Medium range ($1\leq\|i-j\|\leq 5$)	842	177
Long range ($\|i-j\|\geq 5$) intra domain	218	77
Interdomain	444	
Total	3152	844
Dihedral restraints[a] $\phi+\psi$	39 + 39	46 + 46
Hydrogen bonds[b]	56	28
Structural statistics		
No. of NOE violations >0.3 Å	0.03	0
No. of dihedral angle violations >5°	0	0
Ramachandran statistics		
Most favored regions (%)	87.69 ± 2.19	90.69 ± 3.02
Allowed regions (%)	9.91 ± 1.96	7.28 ± 2.84
Generously allowed regions (%)	1.48 ± 0.92	1.42 ± 0.98
Disallowed regions (%)	0.92 ± 0.87	0.58 ± 0.78
WHATIF analysis		
Structure Z-scores		
First generation packing quality	−0.81 ± 0.20	−0.26 ± 0.26
Second generation packing quality	−0.16 ± 0.41	0.67 ± 0.61
Ramachandran plot appearance	−1.29 ± 0.42	−0.88 ± 0.60
χ^{-1}/χ^{-2} rotamer normality	−0.54 ± 0.47	−0.37 ± 0.64
Backbone conformation	−2.56 ± 0.55	−1.73 ± 0.69
Counts		
Average number of bumps	6.97 ± 2.53	1.88 ± 1.30
Average sum of bumps	0.36 ± 0.17	0.08 ± 0.08
Number of bumps per 100 residues	5.62 ± 2.04	2.94 ± 2.03
Unsatisfied buried hydrogen donors	7.72 ± 2.39	4.56 ± 1.83
Unsatisfied buried hydrogen acceptors	0.34 ± 0.48	0.04 ± 0.20
r.m.s. Z-scores		
Bond lengths	0.66 ± 0.02	0.61 ± 0.02
Bond angles	0.81 ± 0.02	0.74 ± 0.02
ω angle restraints	0.59 ± 0.05	0.58 ± 0.04
Side chain planarity	0.74 ± 0.07	0.63 ± 0.14
Improper dihedral distribution	0.82 ± 0.03	0.76 ± 0.04
Inside/outside distribution	1.18 ± 0.02	1.19 ± 0.04
Superposition regions[c]	3–46	4–50
Mean global BB r.m.s. deviation	0.46 ± 0.08	1.02 ± 0.26
Mean global heavy r.m.s. deviation	1.18 ± 0.12	1.90 ± 0.23

[a] Dihedral restraints were generated by TALOS on the basis of backbone atom chemical shifts.
[b] Hydrogen bonds were defined with two distance restraints: 1.8 Å ≤ d(HN–O) ≤ 2.3 and 2.8 Å ≤ d(N–O) ≤ 3.3 Å.
[c] The structures were superimposed on the backbone (BB) atoms of the given regions corresponding to the structured parts.

The different molecular weights of BA1655 and BA5174 observed by analytical ultracentrifugation correlated with different retention volumes of the proteins in size exclusion chromatography (data not shown). BA5174 consistently eluted with a higher retention volume than BA1655 even at loading concentrations (0.5–1 mM) higher than those used in the analytical ultracentrifugation experiments. As the sizes of these proteins are close to the resolution limit of the column, the gel filtration experiments did not allow the molecular weights of the proteins to be determined accurately. However, the elution profiles do suggest that BA1655 is larger than BA5174. These data clearly indicate, that in agreement with the NMR data and over a wide range of protein concentrations and under different solvent conditions, BA1655 is dimeric, whereas BA5174 is monomeric. We infer that the increased line widths in the NMR spectrum of BA5174 at higher temperatures and concentrations reflect a multimeric species. The phenomenon can therefore be considered an artifact of higher protein concentrations.

DISCUSSION

Structural Comparisons—The structure of the BA1655 dimer has obvious similarity to another protein from the sporulation phosphorelay, Spo0B. Spo0B is a two-domain protein with an N-terminal α-helical hairpin and a C-terminal α/β domain (43). The two α-helices of the N-terminal domain form an intermolecular four-helix bundle in the Spo0B dimer (Fig. 6*A*). In the dimer, these helices are in head-to-head apposition rather than the head-to-tail orientation observed in BA1655 (Fig. 6, *A* and *B*). The similarity in structure is nevertheless striking because both Spo0B and the aspartic acid phosphatases participate in phosphotransfer reactions with a common substrate, Spo0A. For Spo0B the phosphoryl group can be reversibly transferred from the conserved His^{30} to Asp^{56} in the active site of the response regulator. In the case of BA1655 and BA5174, the phosphoryl group is thought to be transferred irreversibly from Asp^{56} to water.

The crystal structure of the complex of Spo0B with the response regulator Spo0F (14) (Fig. 6*A*) reveals that interactions between Spo0B and Spo0F are principally mediated via the four-helix bundle with subsidiary contributions from the α/β domain. In the $Spo0B_2$-$Spo0F_2$ complex, the active sites of the Spo0F protomers are buried by the interactions with Spo0B so that the participating atoms in the phosphotransfer chemistry, His^{30} Nϵ of Spo0B and Asp^{54} Oδ of Spo0F, are separated by 4.9 Å. The side chain amide of Asn^{34} of Spo0B, situated one helical turn from the acceptor histidine, is well placed to contribute to the phosphotransfer process.

A relevant comparison can also be made with the chemotaxis protein CheZ. Like the Spo0E-like proteins, CheZ is a phosphatase that dephosphorylates a response regulator protein, in this case CheY~P. The structure of the complex between CheZ and CheY (Fig. 6*C*) has been solved from crystals grown in the presence of BeF_3^-, a phosphoryl group mimic (44). Like BA1655 and BA5174, the structure of CheZ is dominated by two α-helices joined by a hairpin turn. In CheZ, these helices are spectacularly long, spanning 105 Å. As in Spo0B and BA1655, they mediate the formation of a dimer. The orientation of the helical pairs is head-to-head as seen in Spo0B rather than head-to-tail as seen in BA1655. The orientation of the pair of response regulator protomers with respect to the helical bundle in the $CheY_2$-$CheZ_2$ complex resembles that seen in the $Spo0F_2$-$Spo0B_2$ complex. The side chain of Gln^{147} of CheZ is inserted into the active site of CheY and coordinates a magnesium ion whose other ligands include the BeF_3^- moiety and the side chains of Asp^{13} and Asp^{57} of CheY. One helical turn away, Asp^{143} of CheZ forms an ionic interaction with Lys^{109} of CheY.

Two other phosphatases, CheC and CheX from *Thermotoga maritima*, which act on CheY, have different structures (45) featuring extensive β-sheets that wrap around exposed α-helices. Although the structures of complexes with CheY are not known, a pair of catalytic residues (Glu^{13} and Asn^{16} in CheC) have been identified by site-directed mutagenesis, and these map to one of a pair of long adjacent helices. They are separated by one turn of the helix. The use of an α-helix to project a pair of polar side chains into the active site of a response regulator seems therefore to be a recurrent theme in protein-aspartate-phosphate phosphotransferases.

Interactions of BA5174 and BA1655 with Spo0A~P—The crystal structure of the receiver domain of Spo0A from *B. stearothermophilus* in the phosphorylated state (10) shows that

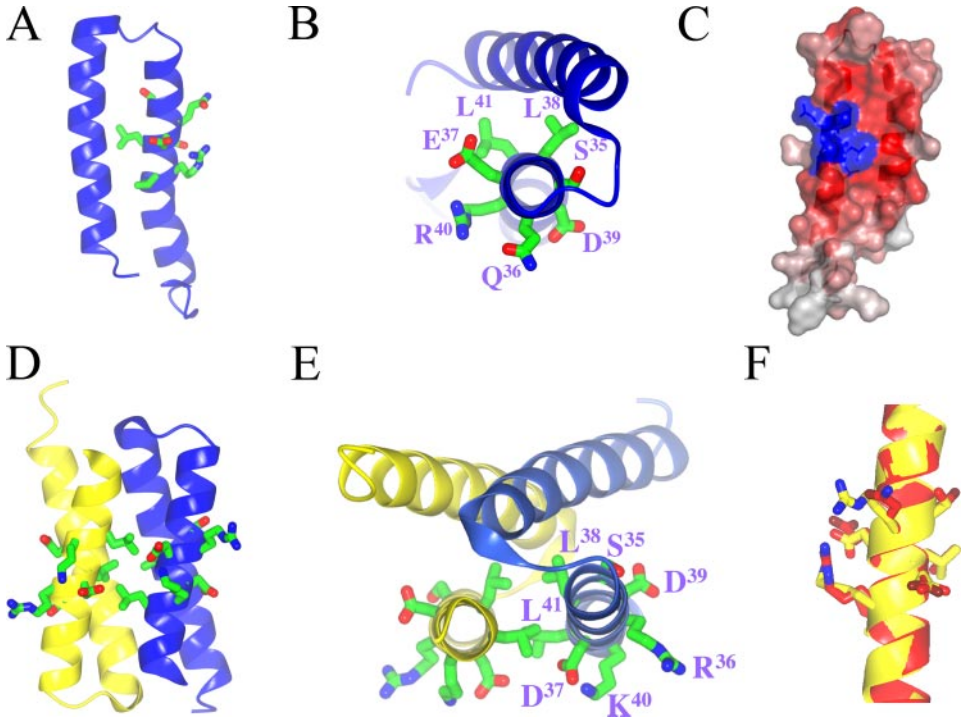

FIGURE 4. **The conserved motifs of BA1655 and BA5174.** *A* and *B*, ribbon representations of BA5174 with the side chains of the residues of the SQELDRL motif shown and colored by atom type. *C*, surface rendering of BA5174 with the conserved motif highlighted in *blue* and the extent of residue conservation represented by the depth of *red* coloring as determined in the program CONSURF (52). This conservation relates to a multiple sequence alignment of ~50 homologs identified from a BLAST search (European Bioinformatics Institute) using the BA5174 sequence. *D* and *E*, orthogonal views of the BA1655 dimer with the chains presented as ribbons and colored in *blue* and *yellow* and the side chains of the residues of the SRDLDKL motif (labeled in one subunit in *E*) shown and colored by atom type. *F*, overlay of the conserved motifs in BA5174 (*red*) and a subunit of BA1655 (*yellow*). *A–E* were made in CCP4MG (53), and *F* was made using PyMOL (48).

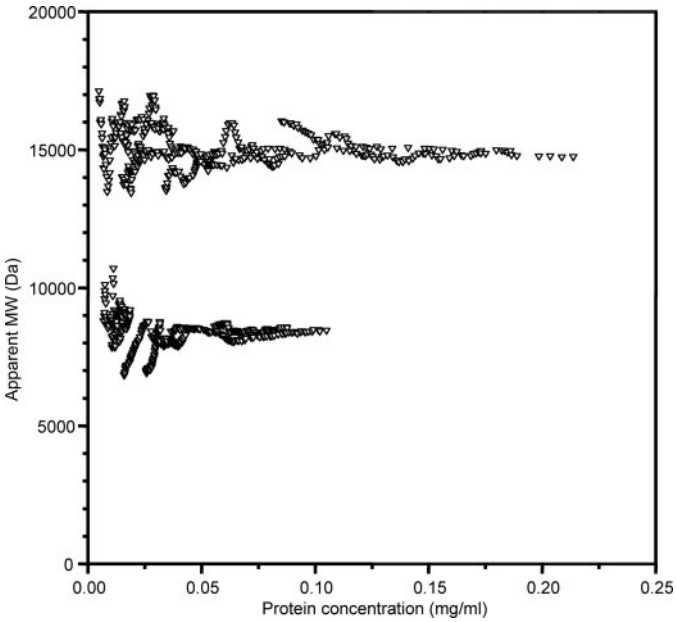

FIGURE 5. **Analytical ultracentrifugation studies.** Shown are plots of apparent molecular mass *versus* concentration for BA5174 (*lower set*) and BA1655 (*upper set*) from centrifugation runs at 25,000 and 35,000 rpm at 20 °C.

the phosphorylated Asp^{56} is situated at the C terminus of the third β-strand of a $(\beta\alpha)_5$ structure and surrounded by loops connecting β-strands to α-helices. The phosphate and its associated divalent cation (Ca^{2+} in the crystal) form a system of interactions with Asp^{9}, Asp^{10}, Thr^{84}, and Lys^{106}; these residues together with Asp^{56} are the most highly conserved in response regulators. In other response regulators the activated structure can be mimicked by BeF_3^- binding, and structural studies show a similar pattern of interactions between the protein and the Mg^{2+}-BeF_3^- moiety (46).

The resemblance to Spo0B and CheZ and the similar structures of the receiver domains of all response regulators suggest that the Spo0E-like phosphatases may form complexes with their partner (Spo0A~P) in a similar manner. The Spo0E interaction surface on Spo0A from *B. subtilis* has been defined in a mutagenesis study (47), which implicated residues Asn^{12}, Pro^{60}, Leu^{62}, and Phe^{88} situated on loops β1-α1, β3-α3, and β4-α4 that surround the active site (Fig. 6*D*). These residues are conserved in Spo0A from *B. stearothermophilus* and *B. anthracis* (15).

The complex of BA1655 with Spo0A~P cannot have the same arrangement as that of CheY-CheZ. This is because the 2-fold symmetry axis runs parallel to the long axis of the helical bundle in CheZ and perpendicular to it in BA1655 (Fig. 6, *B* and *C*). This places the SRDLD*X*L motifs adjacent on one face of the dimer in BA1655, whereas the active residues in CheZ are diametrically opposite one another in the dimer. Unlike CheY~P and Spo0F~P, which are monomeric, Spo0A~P is a dimer in which the receiver domains are expected to be related by a 2-fold rotational symmetry (40). Although this symmetry is compatible with that of the BA1655 dimer, it is not obvious on steric grounds that both active sites of a Spo0A~P dimer could simultaneously engage the conserved motifs of the BA1655 dimer. Clearly this is not obligatory for activity because BA5174, which also dephosphorylates Spo0A~P, is a monomer.

It is possible that the complexes that BA1655 and BA5174 form with Spo0A~P differ because there are sequence variations within the motifs, and the structural context of the motif differs at the tertiary and quaternary level. As a result, our attempts to use simple docking approaches to generate complexes of these proteins with N-Spo0A~P have not produced compelling, or even plausible, models.

Mechanistic Considerations—Response regulators can autodephosphorylate, suggesting the possibility that the cognate phosphatases act by augmenting the efficiency of this reaction in a manner reminiscent of the action of GTPase-activating proteins (GAPs). In GAP-GTPase complexes, residues termed arginine fingers or asparagine thumbs from the GAPs are

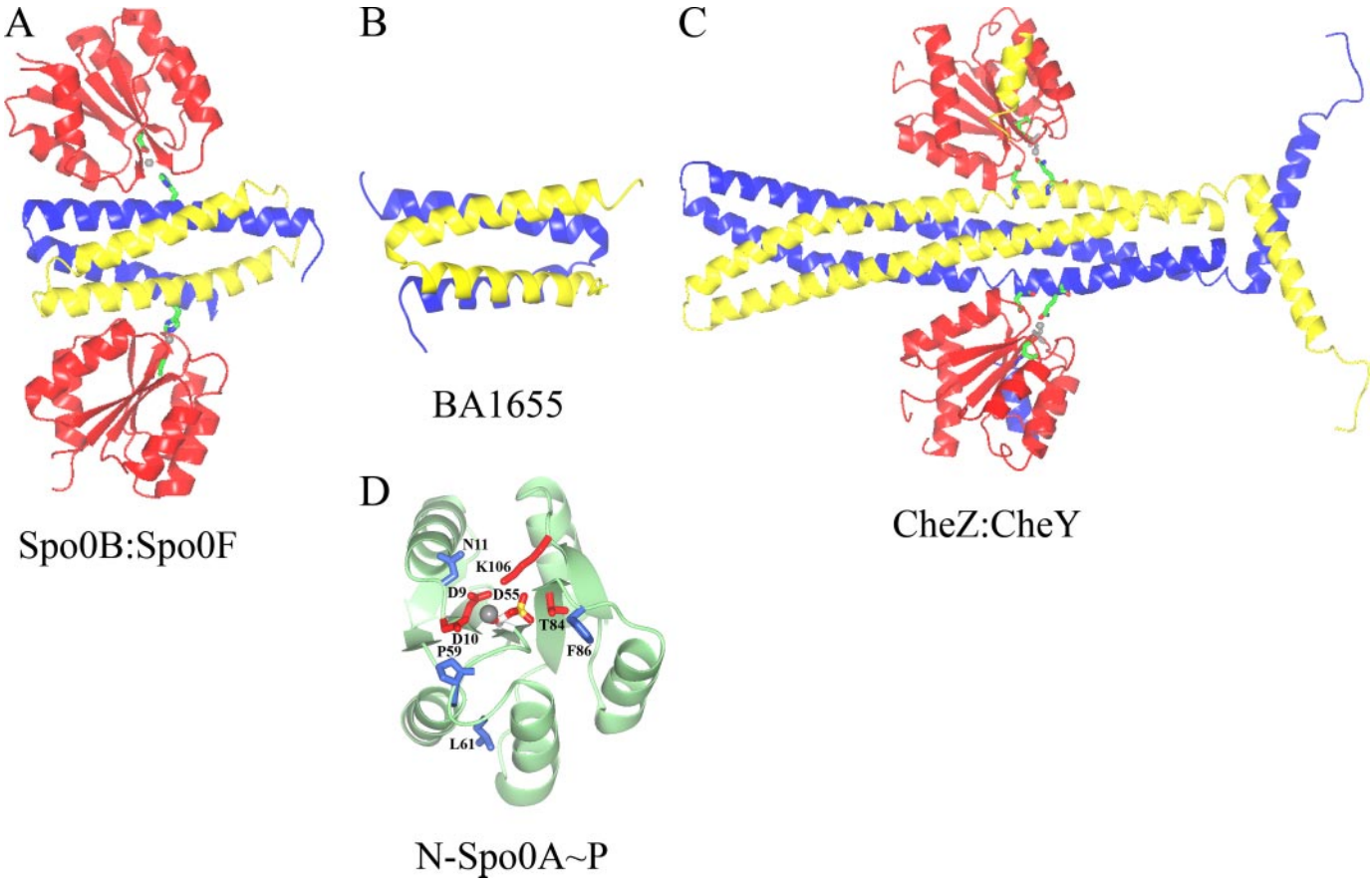

FIGURE 6. **Structure comparisons.** *A*, ribbon diagram of the Spo0B-Spo0F complex. In the Spo0B protomers (colored *yellow* and *blue*) the C-terminal α/β domains have been omitted for clarity. The Spo0F molecules are in *red*. The side chains of the phosphorylatable aspartates Asp^{54} and histidines His^{30} in Spo0F and Spo0B, respectively, are shown in *cylinder* representation with the bound Mg^{2+} atoms drawn as *gray spheres*. *B*, ribbon diagram of the BA1655 dimer with chains colored in *blue* and *yellow*. *C*, ribbon diagram of the CheZ-CheY complex with the CheZ subunits in *yellow* and *blue* and the CheY in *red*. Asp^{57}-BeF_3 from CheY and Asp^{143} and Gln^{147} from CheZ are shown in *licorice* representation. *D*, ribbon representation of N-Spo0A~P looking into the active site. The atoms of the aspartate phosphate side chain are colored by element while conserved side chains of the active site are colored in *red* with the divalent metal ion in *gray*. Residues that have been shown to interact with Spo0E in *B. subtilis* are shown in *blue*. The figure panels were made using CCP4MG (53).

inserted into the GTP-binding site of the GTPase, providing guanidine and amide groups, respectively, which contribute to catalysis of GTP hydrolysis (49). It may be no coincidence that in BA5174 the amide group of Gln^{36}, which is predicted to approach the phosphorylated Asp, can be replaced by the guanidino group of Arg^{36} in BA1655.

For aspartate phosphate dephosphorylation in response regulators, the accepted reaction mechanism involves in-line attack of a water molecule on the phosphorus atom of the phosphoryl group generating a pentavalent transition state that collapses with breakage of the phosphorus-carboxylate oxygen bond. This reaction has similarities to GTP hydrolysis and by analogy with the GAPs, the Gln/Arg^{36} residues may variously contribute to catalysis by reorganizing the active site stereochemistry in Spo0A, by positioning the nucleophilic water molecule, or by stabilizing the charge accumulating in the transition state. The conserved Asp^{39} may facilitate these events by forming ionic interactions with the conserved Lys^{106} of Spo0A in an analogous way to the interaction of Asp^{143} of CheZ with Lys^{109} of CheY (44). However, these proposals are highly speculative, and the details of the interactions between the sporulation response regulators and their phosphatase partners as well as the reaction mechanism will only be unraveled by further experiment.

Concluding Remarks—The NMR structures of BA1655 and BA5174 reveal subunits composed of two α-helices joined by a tight turn and an extended disordered segment at the C terminus. The presence of the disordered C-terminal segment probably accounts for our failure to obtain crystals of this protein. In the archetypal Spo0A phosphatase, Spo0E from *B. subtilis*, there is a C-terminal extension of ~25 residues relative to BA1655 and BA5174. These residues are probably functionally important because (i) a *B. subtilis* strain harboring *spo0E11*, which encodes Spo0E with a 14-residue truncation at the C terminus, is defective in sporulation and (ii) the purified Spo0E11 protein is 5-fold more active as a phosphatase than wild type Spo0E. The latter observation implies an inhibitory role for the C-terminal residues in wild type Spo0E.

The different quaternary structures of BA1655 and BA5174 were unexpected and emphasize the versatility of molecular interactions among the proteins of the sporulation phosphorelay. The response regulator modules of Spo0F and Spo0A form productive phosphotransferase interactions with helical bundles presented in the form of a monomeric protein (BA5174), a head-to-tail dimeric protein (BA1655), and a head-to-head dimeric protein (Spo0B). The work described here extends the structural characterization of the sporulation phosphorelay,

which together with complementary studies of chemotaxis systems has established stereochemical insights into recognition and catalysis in two-component systems.

Acknowledgments—We thank Andrew Leech (University of York, York, UK) for analytical ultracentrifugation analysis, Alexandre Bonvin for help setting up dimer calculations, and Richard Lewis (University of Newcastle, Newcastle, UK) for providing phosphorylated protein.

REFERENCES

1. Piggot, P. J., and Coote, J. G. (1976) *Bacteriol. Rev.* **40,** 908–962
2. Piggot, P. J., and Hilbert, D. W. (2004) *Curr. Opin. Microbiol.* **7,** 579–586
3. Burbulys, D., Trach, K. A., and Hoch, J. A. (1991) *Cell* **64,** 545–552
4. Jiang, M., Shao, W., Perego, M., and Hoch, J. A. (2000) *Mol. Microbiol.* **38,** 535–542
5. LeDeaux, J. R., and Grossman, A. D. (1995) *J. Bacteriol.* **177,** 166–175
6. Kobayashi, K., Shoji, K., Shimizu, T., Nakano, K., Sato, T., and Kobayashi, Y. (1995) *J. Bacteriol.* **177,** 176–182
7. Perego, M., Hanstein, C., Welsh, K. M., Djavakhishvili, T., Glaser, P., and Hoch, J. A. (1994) *Cell* **79,** 1047–1055
8. Ohlsen, K. L., Grimsley, J. K., and Hoch, J. A. (1994) *Proc. Natl. Acad. Sci. U. S. A.* **91,** 1756–1760
9. Perego, M. (2001) *Mol. Microbiol.* **42,** 133–143
10. Lewis, R. J., Brannigan, J. A., Muchova, K., Barak, I., and Wilkinson, A. J. (1999) *J. Mol. Biol.* **294,** 9–15
11. Madhusudan, Zapf, J., Whiteley, J. M., Hoch, J. A., Xuong, N. H., and Varughese, K. I. (1996) *Structure* (*Lond.*) **4,** 679–690
12. Perego, M., and Brannigan, J. A. (2001) *Peptides* **22,** 1541–1547
13. Perego, M. (1997) *Proc. Natl. Acad. Sci. U. S. A.* **94,** 8612–8617
14. Zapf, J., Sen, U., Madhusudan, Hoch, J. A., and Varughese, K. I. (2000) *Structure* (*Lond.*) **8,** 851–862
15. Stephenson, K., and Hoch, J. A. (2002) *Mol. Microbiol.* **46,** 297–304
16. Brunsing, R. L., La Clair, C., Tang, S., Chiang, C., Hancock, L. E., Perego, M., and Hoch, J. A. (2005) *J. Bacteriol.* **187,** 6972–6981
17. Folkers, G. E., van Buuren, B. N. M., and Kaptein, R. (2004) *J. Struct. Funct. Genomics* **5,** 119–131
18. Jansson, M., Li, Y. C., Jendeberg, L., Anderson, S., Montelione, B. T., and Nilsson, B. (1996) *J. Biomol. NMR* **7,** 131–141
19. Sattler, M., Schleucher, J., and Griesinger, C. (1999) *Prog. Nucl. Magn. Reson. Spectrosc.* **34,** 93–158
20. Whitehead, B., Tessari, M., Düx, P., Boelens, R., Kaptein, R., and Vuister, G. W. (1997) *J. Biomol. NMR* **9,** 313–316
21. Goddard, T. D., and Kneller, D. G. (2006) *SPARKY 3*, University of California, San Francisco
22. Leutner, M., Gschwind, R. M., Lermann, J., Schwarz, C., Gemmecker, G., and Kessler, H. (1998) *J. Biol. NMR* **11,** 31–43
23. Zimmerman, D. E., Kulikowski, C. A., Huang, Y., Feng, W., Tashiro, M., Shimotakahara, S., Chien, C., Powers, R., and Montelione, G. T. (1997) *J. Mol. Biol.* **269,** 592–610
24. Diercks, T., Coles, M., and Kessler, H. (1999) *J. Biomol. NMR* **15,** 177–180
25. Herrmann, T., Guntert, P., and Wüthrich, K. (2002) *J. Mol. Biol.* **319,** 209–227
26. Güntert, P., Mumenthaler, C., and Wüthrich, K. (1997) *J. Mol. Biol.* **273,** 283–298
27. Cornilescu, G., Delaglio, F., and Bax, A. (1999) *J. Biomol. NMR* **13,** 289–302
28. Brunger, A. T., Adams, P. D., Clore, G. M., Delano, W. L., Gros, P., Grosse-Kunstleve, R. W., Jiang, J.-S., Kuszewski, J., Nilges, M., Pannu, N. S., Read, R. J., Rice, L. M., Simonson, T., and Warren, G. L. (1997–2001) *Crystallography & NMR System* (*CNS*), Version 1.1, Yale University, New Haven, CT
29. Nederveen, A. J., Doreleijers, J. F., Vranken, W., Miller, Z., Spronk, C. A., Nabuurs, S. B., Guntert, P., Livny, M., Markley, J. L., Nilges, M., Ulrich, E. L., Kaptein, R., and Bonvin, A. M. (2005) *Proteins* **59,** 662–672
30. Vriend, G. (1990) *J. Mol. Graph.* **8,** 52–56
31. Morris, A. L., MacArthur, M. W., Hutchinson, E. G., and Thornton, J. M. (1992) *Proteins* **12,** 345–364
32. Laskowski, R. A., MacArthur, M. W., Moss, D. S., and Thornton, J. M. (1993) *J. Appl. Crystallogr.* **26,** 283–291
33. Arantes, O., and Lereclus, D. (1991) *Gene* (*Amst.*) **108,** 115–119
34. Koehler, T. M., Dai, Z., and Kaufman-Yarbray, M. (1994) *J. Bacteriol.* **176,** 586–595
35. Schaeffer, P., Millet, J., and Aubert, J. P. (1965) *Proc. Natl. Acad. Sci. U. S. A.* **54,** 704–711
36. Poyart, C., and Trieu-Cuot, P. (1997) *FEMS Microbiol. Lett.* **156,** 193–198
37. Ferrari, E., Howard, S. M., and Hoch, J. A. (1986) *J. Bacteriol.* **166,** 173–179
38. Muchová, K., Lewis, R. J., Perečko, D., Brannigan, J. A., Ladds, J. C., Leech, A., Wilkinson, A. J., and Barák, I. (2004) *Mol. Microbiol.* **53,** 829–842
39. Zapf, J. W., Hoch, J. A., and Whiteley, J. M. (1996) *Biochemistry* **35,** 2926–2933
40. Lewis, R. J., Scott, D. J., Brannigan, J. A., Ladds, J. C., Cervin, M. A., Spiegelman, G. B., Hoggett, J. G., Barák, I., and Wilkinson, A. J. (2002) *J. Mol. Biol.* **316,** 235–245
41. Perego, M., and Hoch, J. A. (1991) *J. Bacteriol.* **173,** 2514–2520
42. Lo Conte, L., Chothia, C., and Janin, J. (1999) *J. Mol. Biol.* **285,** 2177–2198
43. Varughese, K. I., Madhusudan, Zhou, X. Z., Whiteley, J. M., and Hoch, J. A. (1998) *Mol. Cell* **2,** 485–493
44. Zhao, R., Collins, E. J., Bourret, R. B., and Silversmith, R. E. (2002) *Nat. Struct. Biol.* **9,** 570–575
45. Park, S. Y., Chao, X., Gonzalez-Bonet, G., Beel, B. D., Bilwes, A. M., and Crane, B. R. (2004) *Mol. Cell* **16,** 563–574
46. Lee, S. Y., Cho, H. S., Pelton, J. G., Yan, D., Henderson, R. K., King, D. S., Huang, L., Kustu, S., Berry, E. A., and Wemmer, D. E. (2001) *Nat. Struct. Biol.* **8,** 52–56
47. Stephenson, S. J., and Perego, M. (2002) *Mol. Microbiol.* **44,** 1455–1467
48. DeLano, W. L. (2002) *The PyMOL Molecular Graphics System*, DeLano Scientific LLC, South San Francisco, CA
49. Daumke, O., Weyand, M., Chakrabarti, P. P., Vetter, I. R., and Wittinghofer, A. (2004) *Nature* **429,** 197–201
50. Gouet, P., Courcelle, E., Stuart, D. I., and Metoz, F. (1999) *Bioinformatics* **15,** 305–308
51. Koradi, R., Billeter, M., and Wuthrich, K. (1996) *J. Mol. Graph* **14,** 51–55
52. Landau, M., Mayrose, I., Rosenberg, Y., Glaser, F., Martz, E., Pupko, T., and Ben-Tal, N. (2005) *Nucleic Acids Res.* **33,** W299–W302
53. Potterton, L., McNicholas, S., Krissinel, E., Gruber, J., Cowtan, K., Emsley, P., Murshudov, G. N., Cohen, S., Perrakis, A., and Noble, M. (2004) *Acta Crystallogr. Sect. D Biol. Crystallogr.* **60,** 2288–2294